Letter Vol. 43, No. 6 / 15 March 2018 / Optics Letters 1395

Optics Letters

Coherent pseudo-mode representation of partially coherent surface plasmon polaritons

Haidan Mao,[1,2] Yahong Chen,[3,4,5] Sergey A. Ponomarenko,[1,6] and Ari T. Friberg[3]

[1]Department of Electrical and Computer Engineering, Dalhousie University, Halifax, Nova Scotia B3J 2X4, Canada
[2]School of Science, Hangzhou Dianzi University, Hangzhou 310018, China
[3]Institute of Photonics, University of Eastern Finland, P.O. Box 111, FI-80101 Joensuu, Finland
[4]College of Physics, Optoelectronics and Energy, Soochow University, Suzhou 215006, China
[5]e-mail: hon2019@163.com
[6]e-mail: serpo@dal.ca

Received 29 January 2018; revised 13 February 2018; accepted 17 February 2018; posted 20 February 2018 (Doc. ID 320772); published 14 March 2018

We develop a general coherent (pseudo)-mode representation of partially coherent surface plasmon polaritons in the Kretschmann excitation geometry. We obtain explicit analytical results for coherent pseudo-modes of narrowband SPPs with Gaussian spectra and spectral correlations. We also evaluate the global degree of coherence of such SPPs which quantifies their overall coherence state within a given spatial domain. Not only will the developed coherent pseudo-mode representation facilitate SPP coherence state characterization, but it will also substantially reduce the computational complexity of the studies of partially coherent SPP interactions with nanoparticles.

OCIS codes: (030.1640) Coherence; (030.1670) Coherent optical effects; (240.6680) Surface plasmons.

https://doi.org/10.1364/OL.43.001395

Surface plasmon polaritons (SPPs) have recently emerged as a workhorse of a thriving research field of plasmonics [1] with a number of promising multidisciplinary connections to other branches of optical physics [2–7]. Recently, there has been growing appreciation of the role the SPP spatial coherence plays in controlling plasmon spatial, spectral, and polarization distributions [8–10]; therefore, the coherence-customized SPPs are expected to serve as versatile tools in numerous multidisciplinary applications [11–15]. To this end, a general theoretical framework was established to describe polychromatic, partially coherent SPPs in the Kretschmann excitation geometry [16] and to demonstrate how nontrivial, structured polychromatic SPP fields can be excited there [17].

The coherent mode representation of partially coherent optical fields [18] helps gain insight into their complicated space–time behavior and is often instrumental in discovering the novel classes of such fields [19–21]. Whenever the true orthonormal coherent modes cannot be simply determined, nonorthogonal pseudo-modes [22–24] can serve in their stead; such pseudo-modes have substantially facilitated recent discovery [25], theoretical description [24,26], and experimental realization [27] of several new classes of volume partially coherent optical beams and pulses. To the best of our knowledge, however, neither the coherent mode nor the pseudo-mode representation of partially coherent *surface* electromagnetic fields has been studied to date.

In this Letter, we put forward a general coherent pseudo-mode decomposition of SPPs in the Kretschmann SPP coupling geometry. We present explicit analytical expressions for the coherent pseudo-modes and their power factors for the case of quasimonochromatic SPPs with Gaussian spectra and Gaussian spectral correlations. We also evaluate the global degree of coherence of such Gaussian Schell-model (GSM) SPPs. Our results shed light on the SPP coherence distribution in one of the most fundamental coupling configurations in plasmonics.

We begin by considering a partially coherent SPP field, excited in the Kretschmann configuration [1] by a TM-polarized, polychromatic light beam with tailored coherence properties (see Fig. 1). In the Kretschmann excitation geometry, a homogenous, isotropic, and nonmagnetic metal film is deposited on a glass prism situated in the xy plane. We take the x axis along the SPP propagation direction and assume that the planar metal–air interface coincides with $z = 0$. A polychromatic electric

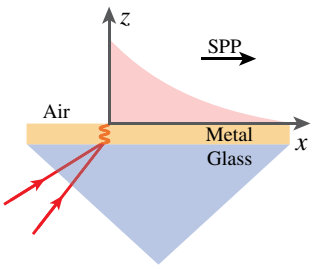

Fig. 1. Illustrating partially coherent SPP field excitation in the Kretschmann configuration.

field realization of the partially coherent SPP field ensemble in the air, at a space–time point $(\mathbf{r}, t)$, then reads [16]

$$\mathbf{E}(\mathbf{r}, t) = \int_{\omega_-}^{\omega_+} E(\omega)\hat{\mathbf{p}}(\omega)\mathrm{e}^{\mathrm{i}[\mathbf{k}(\omega)\cdot\mathbf{r}-\omega t]}\mathrm{d}\omega, \tag{1}$$

where $\omega_\pm$ specifies the SPP frequency bandwidth, $E(\omega)$ stands for a complex random spectral amplitude at the origin ($\mathbf{r} = 0$), and

$$\mathbf{k}(\omega) = k_x(\omega)\hat{\mathbf{e}}_x + k_z(\omega)\hat{\mathbf{e}}_z, \tag{2}$$

$$\hat{\mathbf{p}}(\omega) = [\mathbf{k}(\omega) \times \hat{\mathbf{e}}_y]/|\mathbf{k}(\omega)|, \tag{3}$$

are the wave and unit polarization vectors, respectively. Here $\hat{\mathbf{e}}_x$, $\hat{\mathbf{e}}_y$, and $\hat{\mathbf{e}}_z$ are the Cartesian unit vectors. For simplicity, we assume that the metal film is thick enough so that mode coupling across the metal can be neglected [28], whereby the components of the SPP wave vector at the metal–air interface in Eq. (2) are given by

$$k_x(\omega) = \frac{\omega}{c}\sqrt{\frac{\epsilon_r(\omega)}{\epsilon_r(\omega)+1}}, \qquad k_z(\omega) = \frac{\omega}{c}\sqrt{\frac{1}{\epsilon_r(\omega)+1}}, \tag{4}$$

where c is the speed of light in vacuum, and $\epsilon_r(\omega)$ denotes the complex-valued relative permittivity of the metal.

The second-order statistical properties of a partially coherent SPP field can be specified by the electric correlation matrix [29], which is obtained by averaging over an ensemble of the field realizations at two space–time points, i.e., $\mathbf{\Gamma}(\mathbf{r}_1, t_1; \mathbf{r}_2, t_2) = \langle \mathbf{E}^*(\mathbf{r}_1, t_1)\mathbf{E}^{\mathrm{T}}(\mathbf{r}_2, t_2)\rangle$. Here the asterisk, superscript T, and the angle brackets denote complex conjugation, matrix transpose, and ensemble average, respectively. It follows from Eqs. (1)–(3) that

$$\mathbf{\Gamma}(\mathbf{r}_1, t_1; \mathbf{r}_2, t_2) = \int_{\omega_-}^{\omega_+}\int_{\omega_-}^{\omega_+} W(\omega_1, \omega_2)\hat{\mathbf{p}}^*(\omega_1)\hat{\mathbf{p}}^{\mathrm{T}}(\omega_2) \times \mathrm{e}^{-\mathrm{i}[\mathbf{k}^*(\omega_1)\cdot\mathbf{r}_1 - \mathbf{k}(\omega_2)\cdot\mathbf{r}_2]}\mathrm{e}^{\mathrm{i}(\omega_1 t_1 - \omega_2 t_2)}\mathrm{d}\omega_1\mathrm{d}\omega_2, \tag{5}$$

where

$$W(\omega_1, \omega_2) = \langle E^*(\omega_1)E(\omega_2)\rangle \tag{6}$$

is an SPP spectral correlation function. The function $W(\omega_1, \omega_2)$ determines the second-order SPP statistical properties, including spectral and spatial distribution, energy flow, the polarization state, and two-point spatio-temporal coherence of the SPP fields [16,17]. It is shown in [16] how $W(\omega_1, \omega_2)$ is related to the second-order spectral and angular correlation function of an electromagnetic source beam exciting polychromatic SPPs in the Kretschmann configuration. We also demonstrated elsewhere that $W(\omega_1, \omega_2)$ and, hence, the second-order field correlations of statistically stationary SPPs can be recovered from far-field measurements [30].

To develop a coherent, in general pseudo-mode, representation of a generic $\mathbf{\Gamma}(\mathbf{r}_1, t_1; \mathbf{r}_2, t_2)$, we start by expanding the SPP spectral correlation function $W(\omega_1, \omega_2)$ in terms of coherent modes as

$$W(\omega_1, \omega_2) = \sum_n \beta_n \varphi_n^*(\omega_1)\varphi_n(\omega_2), \tag{7}$$

where $\{\beta_n\}$ are real and nonnegative eigenvalues of the linear Fredholm integral equation [18], and the corresponding eigenmodes $\{\varphi_n(\omega)\}$ form an orthonormal set so that

$$\int_{\omega_-}^{\omega_+} \varphi_m^*(\omega)\varphi_n(\omega)\mathrm{d}\omega = \delta_{mn}. \tag{8}$$

It follows at once on substituting from Eq. (7) into Eq. (5) after a rearrangement that the SPP field correlation matrix can be represented as

$$\mathbf{\Gamma}(\mathbf{r}_1, t_1; \mathbf{r}_2, t_2) = \sum_n \nu_n \mathbf{\Phi}_n^*(\mathbf{r}_1, t_1)\mathbf{\Phi}_n^{\mathrm{T}}(\mathbf{r}_2, t_2), \tag{9}$$

where we have introduced a set of normalized vector modes $\{\mathbf{\Phi}_n(\mathbf{r}, t)\}$ as

$$\mathbf{\Phi}_n(\mathbf{r}, t) = \frac{\mathbf{\Theta}_n(\mathbf{r}, t)}{\left[\int_{-\infty}^{+\infty}\int_D \mathbf{\Theta}_n^{\mathrm{T}}(\mathbf{r}, t)\mathbf{\Theta}_n^*(\mathbf{r}, t)\mathrm{d}^2\mathbf{r}\mathrm{d}t\right]^{1/2}}, \tag{10}$$

such that

$$\int_{-\infty}^{+\infty}\int_D \mathbf{\Phi}_n^{\mathrm{T}}(\mathbf{r}, t)\mathbf{\Phi}_n^*(\mathbf{r}, t)\mathrm{d}^2\mathbf{r}\mathrm{d}t = 1, \tag{11}$$

with D being the spatial SPP excitation volume, and the modal weights $\{\nu_n\}$ as

$$\nu_n = \beta_n \int_{-\infty}^{+\infty}\int_D \mathbf{\Theta}_n^{\mathrm{T}}(\mathbf{r}, t)\mathbf{\Theta}_n^*(\mathbf{r}, t)\mathrm{d}^2\mathbf{r}\mathrm{d}t. \tag{12}$$

Here

$$\mathbf{\Theta}_n(\mathbf{r}, t) = \int_{\omega_-}^{\omega_+} \varphi_n(\omega)\hat{\mathbf{p}}(\omega)\mathrm{e}^{\mathrm{i}[\mathbf{k}(\omega)\cdot\mathbf{r}-\omega t]}\mathrm{d}\omega \tag{13}$$

are the unnormalized vector modes. A quick glance at Eq. (13) reveals that due to the presence of SPP losses and a nontrivial dependence of $\mathbf{k}$ on ω, the modes $\{\mathbf{\Phi}_n(\mathbf{r}, t)\}$ are not orthogonal, even though $\{\varphi_n(\omega)\}$ are. Thus, $\{\mathbf{\Phi}_n(\mathbf{r}, t)\}$ are pseudo-modes in the spirit of [22–24]. We stress that these coherent vector pseudo-modes are still uncorrelated, although the orthogonality condition has been relaxed; in particular, the modal weights $\{\nu_n\}$, which specify the fraction of the source energy carried by a given mode, add up to the total energy of the source as a straightforward consequence of Eqs. (9) and (11).

Further, in complete analogy with the volume partially coherent sources, the global degree of coherence of the partially coherent SPPs can be defined as a ratio of the energy carried by the lowest-order mode to the total energy of the SPP source [31,32] as

$$G = \frac{\nu_0}{\sum_{n=0}^{N-1}\nu_n}, \tag{14}$$

where N is an effective number of excited modes. The global degree of coherence is bounded as $0 \le G \le 1$, with the upper and lower limits corresponding to the fully coherent and fully incoherent sources, respectively. Thus, given the orthonormal modes of $W(\omega_1, \omega_2)$, which can be determined, at least in principle, by solving the Fredholm integral equation, Eqs. (9)–(13) furnish the coherent pseudo-mode representation of *any* polychromatic SPP field in the Kretschmann geometry, and Eq. (14) quantifies the overall coherence of the SPP field within the excitation volume.

To illustrate our general results, we consider a GSM for the SPP spectral correlations such that

$$W(\omega_1,\omega_2) = I_0 \exp\left[-\frac{(\omega_1-\omega_0)^2+(\omega_2-\omega_0)^2}{4\sigma_s^2}\right] \times \exp\left[-\frac{(\omega_1-\omega_2)^2}{2\sigma_c^2}\right], \quad (15)$$

where I_0 is a constant, ω_0 is the SPP central frequency, and σ_s and σ_c denote the SPP spectral width and spectral coherence length, respectively. The normalized eigenfunctions and the corresponding eigenvalues of the GSM source are analytically known as [18]

$$\varphi_n(\omega) = \left(\frac{2c_0}{\pi}\right)^{1/4} \frac{1}{(2^n n!)^{1/2}} \times H_n[(\omega-\omega_0)(2c_0)^{1/2}]e^{-c_0(\omega-\omega_0)^2}, \quad (16)$$

and $\beta_n = I_0[\pi/(a_0+b_0+c_0)]^{1/2}[b_0/(a_0+b_0+c_0)]^n$, where $a_0 = (4\sigma_s^2)^{-1}$, $b_0 = (2\sigma_c^2)^{-1}$, and $c_0 = (a_0^2+2a_0b_0)^{1/2}$; H_n is a Hermite polynomial of order n. To simplify our calculations, we further assume that the source is spectrally narrowband such that the metal dispersion can be ignored [16], implying that $\epsilon_r(\omega) \approx \epsilon_r(\omega_0)$. It then follows at once that at this level of approximation the frequency integration ranges in Eqs. (8) and (13) can be extended all the way to infinity. Under these conditions, and on substituting from Eq. (16) into Eq. (13), we obtain the following analytical expressions for the coherent vector pseudo-modes of a GSM SPP:

$$\mathbf{\Theta}_n(\mathbf{r},t) = \hat{\mathbf{p}}(\omega_0)\Theta_n(\mathbf{r},t), \quad (17)$$

with

$$\Theta_n(\mathbf{r},t) = \left(\frac{2\pi}{c_0}\right)^{1/4} \frac{i^n}{(2^n n!)^{1/2}} e^{i[\mathbf{k}(\omega_0)\cdot\mathbf{r}-\omega_0 t]} \times H_n\left[\frac{\mathbf{k}(\omega_0)\cdot\mathbf{r}-\omega_0 t}{\sqrt{2c_0}\omega_0}\right] e^{-[\mathbf{k}(\omega_0)\cdot\mathbf{r}-\omega_0 t]^2/(4c_0\omega_0^2)}. \quad (18)$$

Using Eqs. (10), (12), (17), and (18), we can numerically evaluate the coherent pseudo-modes and the corresponding global degree of coherence for the GSM SPPs.

In Fig. 2, we exhibit the space–time distributions of the first four pseudo-mode functions $\Phi_n(x,t) \equiv \hat{\mathbf{p}}(\omega_0)\cdot\mathbf{\Phi}_n(x,t)$, with $n = 0, 1, 2, 3$, for a narrowband GSM SPP at an Ag–air interface with the SPP central wavelength $\lambda_0 = 653$ nm. It can be inferred from Fig. 2 that each mode remains highly confined over the SPP propagation distance $l_{\mathrm{SPP}}(\lambda_0)$, and the peak amplitude position of each mode experiences a time shift on SPP propagation away from the excitation point. The lateral shift of each mode in the space–time domain in the absence of dispersion arises as a consequence of the mode phase shift in the space–frequency domain, as evidenced by Eqs. (13) and (18). We note in passing that a similar dynamical phase shift was utilized to experimentally generate self-steering partially coherent beams in free space [33]. Further, the mode of order n has exactly n nodes and, thus, appears to be split into $n+1$ lobes.

In Fig. 3, we display the normalized modal weights for GSM SPP at an Ag–air interface as a function of the mode order n for different values of σ_c and σ_s. Figure 3 reveals that the energy carried by each mode decreases monotonously with the mode number n at a rate depending on both σ_c and σ_s. As σ_c decreases or σ_s increases, the SPP field becomes less coherent,

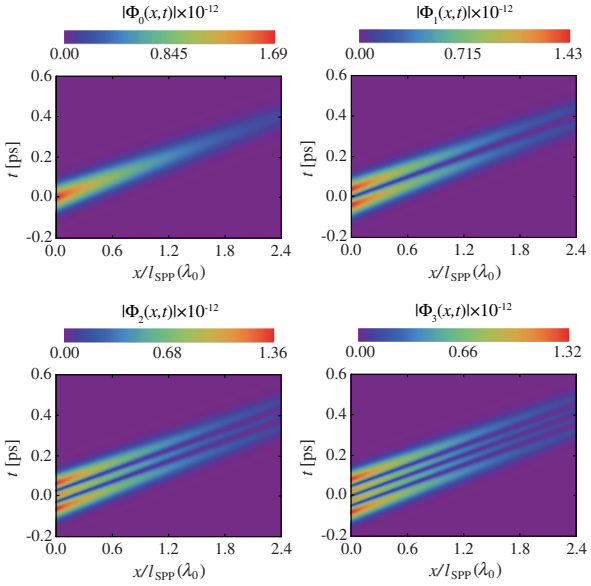

Fig. 2. Space–time distributions of the first four pseudo-mode amplitudes $|\Phi_n(x,t)|$ for a narrowband GSM SPP at an Ag–air interface ($z = 0$) with the central wavelength $\lambda_0 = 653$ nm. The spectral width σ_s and the spectral coherence length σ_c of $W(\omega_1,\omega_2)$ are taken to be $0.02\omega_0$ and $0.004\omega_0$, respectively, where $\omega_0 = 2\pi c/\lambda_0$ is the SPP central frequency. $l_{\mathrm{SPP}}(\lambda_0) = 1/k_x''(\lambda_0)$ is the SPP propagation length, with the double prime denoting an imaginary part. The relative permittivity of Ag is obtained using the empirical data of [34].

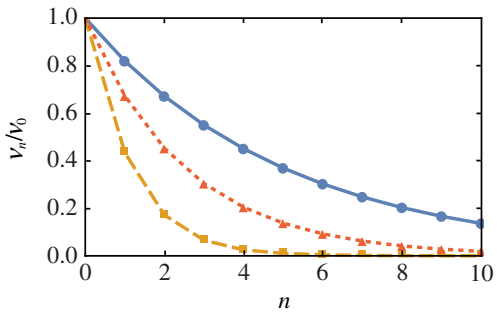

Fig. 3. Normalized modal weights ν_n/ν_0 for a narrowband GSM SPP with the central wavelength $\lambda_0 = 653$ nm as a function of the mode order n at an Ag–air interface. The parameters are $\sigma_s = 0.02\omega_0$, $\sigma_c = 0.004\omega_0$ (blue solid curve), $\sigma_s = 0.02\omega_0$, $\sigma_c = 0.02\omega_0$ (orange dashed curve), $\sigma_s = 0.01\omega_0$, and $\sigma_c = 0.004\omega_0$ (red dotted curve). Here $\omega_0 = 2\pi c/\lambda_0$ is the SPP central frequency. We used the empirical data of [34] to evaluate the relative permittivity of Ag.

so that we have to increase the effective number of excited modes to faithfully represent such a field.

Further, we evaluate the global degree of coherence G of a GSM SPP at an Ag–air interface as a function of σ_c and σ_s, respectively. The results are exhibited in Fig. 4. It is seen from the figure that the global degree of coherence increases with σ_c and decreases with σ_s. Moreover, G tends to zero for spectrally uncorrelated SPPs, $\sigma_c \to 0$, even though the longitudinal coherence length of such SPPs remains on the order of a

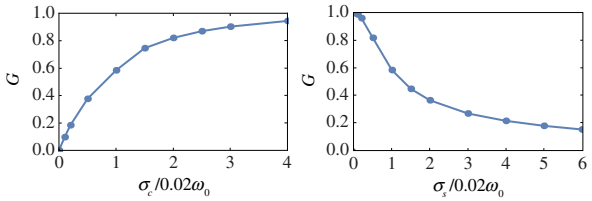

Fig. 4. Global degree of coherence of a narrowband GSM SPP with the central wavelength $\lambda_0 = 653$ nm at an Ag–air interface as a function of the spectral coherence length σ_c (the spectral width σ_s is fixed at $0.02\omega_0$) (left panel), and of the spectral width σ_s (the spectral coherence length is fixed at $0.02\omega_0$) (right panel). Here $\omega_0 = 2\pi c/\lambda_0$ is the SPP central frequency. The relative permittivity of Ag corresponds to the empirical data of [34].

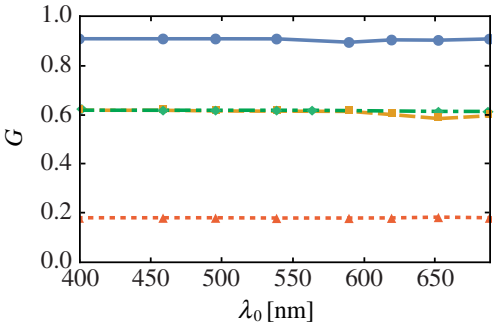

Fig. 5. Global degree of coherence of a narrowband GSM SPP at an Ag–air interface as a function of the central wavelength λ_0 for different spectral coherence lengths σ_c: $\sigma_c = 0.06\omega_0$ (blue solid curve), $\sigma_c = 0.02\omega_0$ (orange dashed curve), $\sigma_c = 0.004\omega_0$ (red dotted curve). The green dashed–dotted curve represents G at an Au–air interface with $\sigma_c = 0.02\omega_0$. The source spectral width σ_s is taken to be $0.02\omega_0$. Here ω_0 is the central frequency at $\lambda_0 = 653$ nm. We use the empirical data from [34] to evaluate the relative permittivities of Ag and Au.

few wavelengths [16]. As monochromatic SPP fields are fully coherent, their global degree of coherence equals unity.

Finally, we demonstrate that G is a robust measure of the overall coherence of narrowband SPPs. In Fig. 5, we display the global degree of coherence of a narrowband GSM SPP as a function of the central wavelength λ_0 at Ag–air and Au–air interfaces for different spectral coherence lengths. It is manifest in the figure that G is virtually independent of the central wavelength λ_0 of narrowband GSM SPPs, thereby making G a convenient quantitative measure of their global coherence properties. We also conclude from Fig. 5 that, at least for conventional plasmonic materials, G is only weakly affected by the metal properties for narrowband SPPs, as seen by comparing the orange dashed and green dashed-dotted curves in Fig. 5.

In conclusion, we have developed a general coherent pseudo-mode representation of polychromatic SPPs in the Kretschmann excitation configuration. We derived explicit analytical expressions for the pseudo-modes and their weight factors for narrowband GSM SPPs and discussed the space–time distributions of a few lower-order pseudo-modes. We also evaluated the global degree of coherence of GSM SPPs which specifies their overall coherence properties within the excitation region. Our results can help to quantitatively characterize the statistical properties of SPPs and to facilitate numerical studies of the partially coherent SPP interactions with nanoparticles in one of the most fundamental excitation geometries in plasmonics.

Funding. Natural Sciences and Engineering Research Council of Canada (NSERC); Academy of Finland (310511); China Scholarship Council (CSC); Hangzhou Dianzi University (HDU).

Acknowledgment. H. Mao thanks the Scholastic Scholarship Fund of Hangzhou Dianzi University, Y. Chen is grateful to the China Scholarship Council (CSC), and S. Ponomarenko is grateful to the Joensuu University Foundation.

REFERENCES

1. S. A. Maier, *Plasmonics: Fundamentals and Applications* (Springer, 2007).
2. A. Boltasseva and H. A. Atwater, Science **331**, 290 (2011).
3. P. Berini and I. De Leon, Nat. Photonics **6**, 16 (2012).
4. M. Kauranen and A. V. Zayats, Nat. Photonics **6**, 737 (2012).
5. A. N. Grigorenko, M. Polini, and K. S. Novoselov, Nat. Photonics **6**, 749 (2012).
6. M. S. Tame, K. R. McEnery, S. K. Özdemir, J. Lee, S. A. Maier, and M. S. Kim, Nat. Phys. **9**, 329 (2013).
7. P. Genevet and F. Capasso, Rep. Prog. Phys. **78**, 024401 (2015).
8. S. Aberra Guebrou, J. Laverdant, C. Symonds, S. Vignoli, and J. Bellessa, Opt. Lett. **37**, 2139 (2012).
9. J. Laverdant, S. Aberra Guebrou, F. Bessueille, C. Symonds, and J. Bellessa, J. Opt. Soc. Am. A **31**, 1067 (2014).
10. A. Norrman, T. Setälä, and A. T. Friberg, Opt. Express **23**, 20696 (2015).
11. E. Ozbay, Science **311**, 189 (2006).
12. D. M. Koller, A. Hohenau, H. Ditlbacher, N. Galler, F. Reil, F. R. Aussenegg, A. Leitner, E. J. W. List, and J. R. Krenn, Nat. Photonics **2**, 684 (2008).
13. S. Aberra Guebrou, C. Symonds, E. Homeyer, J. C. Plenet, Y. N. Gartstein, V. M. Agranovich, and J. Bellessa, Phys. Rev. Lett. **108**, 066401 (2012).
14. A. Bouhelier and G. P. Wiederrecht, Phys. Rev. B **71**, 195406 (2005).
15. W. Liu, D. N. Neshev, A. E. Miroshnichenko, I. V. Shadrivov, and Y. S. Kivshar, Phys. Rev. B **83**, 073404 (2011).
16. A. Norrman, S. A. Ponomarenko, and A. T. Friberg, Europhys. Lett. **116**, 64001 (2016).
17. Y. Chen, A. Norrman, S. A. Ponomarenko, and A. T. Friberg, Phys. Rev. A (2018, submitted).
18. L. Mandel and E. Wolf, *Optical Coherence and Quantum Optics* (Cambridge University, 1995).
19. S. A. Ponomarenko, J. Opt. Soc. Am. A **18**, 150 (2001).
20. S. A. Ponomarenko, W. Huang, and M. Cada, Opt. Lett. **32**, 2508 (2007).
21. A. S. Ostrovsky, J. Garcia-Garcia, C. Rickenstroff-Parrao, and M. A. Olvera-Santamaria, Opt. Lett. **42**, 5182 (2017).
22. S. A. Ponomarenko, Opt. Express **19**, 17086 (2011).
23. R. Martinez-Herrero, P. M. Mejias, and F. Gori, Opt. Lett. **34**, 1399 (2009).
24. S. Yang, S. A. Ponomarenko, and Z. Chen, Opt. Lett. **40**, 3081 (2015).
25. L. Ma and S. A. Ponomarenko, Opt. Lett. **39**, 6656 (2014).
26. L. Ma and S. A. Ponomarenko, Opt. Express **23**, 1848 (2015).
27. Y. Chen, S. A. Ponomarenko, and Y. Cai, Appl. Phys. Lett. **109**, 061107 (2016).
28. A. Norrman, T. Setälä, and A. T. Friberg, Opt. Lett. **38**, 1119 (2013).
29. A. T. Friberg and T. Setälä, J. Opt. Soc. Am. A **33**, 2431 (2016).
30. Y. Chen, A. Norrman, S. A. Ponomarenko, and A. T. Friberg, Opt. Lett. **42**, 3279 (2017).
31. A. Starikov, J. Opt. Soc. Am. **72**, 1538 (1982).
32. M. J. Bastiaans, J. Opt. Soc. Am. A **1**, 711 (1984).
33. Y. Chen, S. A. Ponomarenko, and Y. Cai, Sci. Rep. **7**, 39957 (2017).
34. E. D. Palik, ed., *Handbook of Optical Constants of Solids* (Academic, 1998).